Available online at www.sciencedirect.com
ScienceDirect
Journal of Sound and Vibration 315 (2008) 939–960
JOURNAL OF SOUND AND VIBRATION
www.elsevier.com/locate/jsvi

Vibrations and pull-in instabilities of microelectromechanical von Kármán elliptic plates incorporating the Casimir force

R.C. Batra[a,*], M. Porfiri[b], D. Spinello[c]

[a]Department of Engineering Science & Mechanics, Virginia Polytechnic Institute & State University, Blacksburg, VA 24061, USA
[b]Department of Mechanical & Aerospace Engineering, Polytechnic University, Brooklyn, NY 11201, USA
[c]The Bradley Department of Electrical & Computer Engineering, Virginia Polytechnic Institute & State University, Blacksburg, VA 24061, USA

Received 15 July 2007; received in revised form 24 January 2008; accepted 7 February 2008
Handling Editor: S. Bolton
Available online 26 March 2008

Abstract

We consider the von Kármán nonlinearity and the Casimir force to first develop a reduced-order model for a prestressed clamped elliptic electrostatically actuated microplate, and then use it to study vibrations and pull-in instability. The reduced-order model is derived by taking a family of linearly independent kinematically admissible functions as basis functions for the transverse displacement. The in-plane displacement vector is expressed as the sum of displacements for irrotational and isochoric waves in a two-dimensional medium. The potentials of these two displacement vector fields satisfy an eigenvalue problem analogous to that of transverse vibrations of a linear elastic membrane. Basis functions for the transverse and the in-plane displacements are related by using the nonlinear equation governing the plate's in-plane motion. The reduced-order model is derived from the equation governing the transverse deflection of the plate. Pull-in parameters are found using the displacement iteration pull-in extraction method and by studying small vibrations of the plate about its predeformed configuration. However, the effect of inertia forces on pull-in parameters has not been analyzed. The reduced-order model for a linear elliptic micromembrane is derived as a special case of that for an elliptic plate.

1. Introduction

Electrostatically actuated microelectromechanical systems (MEMS) are used as transistors, switches, micro-mirrors, pressure sensors, micro-pumps, moving valves, and micro-grippers, see for example Refs. [1–4]. An electrostatically actuated MEMS is comprised of a conductive deformable body suspended above a rigid grounded body [5]. An applied direct current (DC) voltage between the two bodies results in the deflection of the deformable body and a consequent change in the system capacitance. When an alternating current is superimposed on the DC voltage to excite harmonic motions of the system, resonant devices are obtained. These devices are used in signal filtering and chemical and mass sensing, see for example Refs. [6–15].

*Corresponding author.
E-mail addresses: rbatra@vt.edu (R.C. Batra), mporfiri@poly.edu (M. Porfiri), dspinell@vt.edu (D. Spinello).

0022-460X/$ - see front matter © 2008 Elsevier Ltd. All rights reserved.
doi:10.1016/j.jsv.2008.02.008

The applied DC voltage has an upper limit beyond which the electrostatic force is not balanced by the elastic restoring force in the deformable conductor. Beyond this critical voltage the deformable conductor snaps and touches the lower rigid plate. This phenomenon, called pull-in instability, has been experimentally observed in Refs. [16,17]. The critical displacement and the critical voltage associated with this instability are called pull-in displacement and pull-in voltage, respectively. Their accurate evaluation is crucial in the design of electrostatically actuated MEMS. In particular, in micro-mirrors [2] and micro-resonators [18], the designer avoids this instability in order to achieve stable motions; while in switching applications [1], the designer exploits this effect to optimize the performance of the device.

For a wide class of electrostatic MEMS, the deformable electrode is a flat body whose thickness h is much smaller than its characteristic in-plane dimension a [19]. Such electrodes can be regarded as two-dimensional plate-like bodies. Since $h/a \ll 1$, an approximate distributed model can be employed, where the system kinematics is described only through the displacement of points on the movable electrode mid-surface, see for example Ref. [20]. Linear and nonlinear microplates have been studied in Refs. [21–24,60]. When the bending stiffness of the deformable electrode is negligible compared to its in-plane stretching stiffness and $g_0/a \ll 1$, where g_0 is the initial gap between the two plates, the electrode can be regarded as a linear elastic membrane. The membrane approximation is valid for $a/h \geqslant 400$, see for example Ref. [25]. Linear elastic micromembranes have been studied in Refs. [26–31]. As discussed in Ref. [26], the plate and the membrane approximations are accurate and reliable for many MEMS such as micro-pumps made of thin glassy polymers and grating light valves comprised of stretched thin ribbons.

With the decrease in device dimensions from the micro to the nanoscale, additional forces on nanoelectromechanical systems (NEMS), such as the Casimir force [32,33] or the van der Waals force [34], should be considered. The Casimir force represents the attraction of two uncharged material bodies due to modification of the zero-point energy associated with the electromagnetic modes in the space between them. The existence of the Casimir force poses a severe constraint on the miniaturization of electrostatically actuated devices. At the nanoscale, the Casimir force may overcome elastic restoring actions in the device and lead to the plates' sticking during the fabrication process. An important feature of the Casimir effect is that, even though its nature is quantistic, it predicts a force between macroscopic bodies.

van der Waals forces are related to electrostatic interaction among dipoles at the atomic scale [34]. Whereas the Casimir force between semi-infinite perfectly conducting parallel plates depends only on the geometry, van der Waals forces depend on material properties of the media. The Casimir force is effective at longer distance than van der Waals forces [34]. van der Waals forces are accounted for in NEMS where interactions occur at the atomic scale, as for example in carbon nanotubes [35]. van der Waals forces are not considered in the work presented below. The effect of van der Waals forces on the pull-in instability of electrostatically actuated microplates has been studied in Ref. [61].

In order to alleviate difficulties associated with the analysis of distributed nonlinear systems, considerable efforts have been devoted to developing reliable reduced-order models for MEMS. A simple lumped spring–mass–system for estimating pull-in parameters has been proposed in Ref. [17], where the elasticity of the deformable body is lumped into the stiffness of a linear spring. The pull-in voltage so obtained usually exceeds that observed experimentally for many applications [36], and the pull-in displacement always equals one-third of the initial gap. Moreover, the aforestated description does not generally incorporate inherent nonlinearities in the restoring forces [4,37]. In Ref. [23], a reduced-order model for microplates that accounts for the mid-plane stretching and the nonlinearity in the electrostatic force has been used to study pull-in instability and natural frequencies of a plate predeformed by an electric field. In Ref. [36], microbeams have been studied through a reduced-order one degree-of-freedom model, which improves the pull-in voltage estimate of the lumped system of Ref. [17]; however, the pull-in displacement is empirically selected. Multimode analysis of microbeams using a nonlinear beam equation has been presented in Refs. [6,38]. In these works, the effect of the number of modes retained in the trial solution on the convergence rate of the reduced-order model is investigated. In Refs. [39,40], a one degree-of-freedom model has been used to extract pull-in parameters and to study the fundamental frequency of a narrow microbeam. This reduced-order model accounts for the mid-plane stretching and fringing fields in the electrostatic load, and it is obtained by taking the function describing the static deflection of the beam under a uniformly distributed load as the trial solution in the Galerkin method. Reduced-order models have also been used to study the sticking phenomenon in

NEMS due to the Casimir force. In Refs. [41,42], a distributed model for a wide microbeam incorporating nonlinear stretching effects has been studied, while in Ref. [43], a lumped one degree-of-freedom model has been used to analyze the stiction phenomenon between two conductors made of different materials. In Ref. [44], the effect of Casimir force on pull-in parameters of NEM switches has been studied using an approximate analytical expression of the critical gap generated through the perturbation theory. A review on applications of proper orthogonal decomposition methods to MEMS analysis can be found in Ref. [45]. The literature on electrostatically actuated MEMS is summarized in Ref. [46].

Here, we derive a reduced-order model for studying static pull-in instability and small vibrations of clamped elliptic microplates predeformed under the combined effects of the Coulomb and the Casimir forces. Elliptic plates are a generalization of circular plates. An advantage of the elliptic shape versus the rectangular one is that stress concentrations usually present at corners of a rectangular plate are absent. In addition, results derived on elliptic geometries can be useful in assessing the effect of geometrical defects on commonly used circular shapes. Also, an elliptic plate has higher fundamental frequency than the circular plate of the same area. Thus, for sensing applications [3,47,48], it may have higher sensitivity to applied disturbances.

Following Ref. [49], we use the large transverse displacement-small strains plate theory [50] by incorporating the von Kármán nonlinearity in the mechanical model. Since small strains are involved, we use the parallel plate approximation for the Coulomb force and the proximity force approximation for the Casimir force. Both these approximations are consistent with the assumption of locally parallel conductors. Thus, the dependence of the Coulomb and the Casimir forces on the spatial derivatives of the gap g is neglected. Fringing fields in the electrostatic force are also discarded. We use the Galerkin method to reduce the governing two-dimensional nonlinear initial-boundary-value problem to a system of nonlinear coupled ordinary differential equations. Static pull-in parameters are computed from the derived reduced-order model by neglecting the inertia forces, and by solving a nonlinear algebraic problem in which both the pull-in voltage and the pull-in displacement are treated as unknowns. For different equilibrium states up to pull-in, the fundamental frequency of the statically deformed plate is obtained by solving the eigenvalue problem related to small vibrations about the equilibrium position. We show that the fundamental frequency goes to zero as pull-in conditions are approached and that the pull-in parameters derived using this technique agree well with those obtained from the static analysis. Reduced-order models for linear elliptic membranes are obtained as special cases of those for the corresponding elliptic plates. To our knowledge, the pull-in instability of a von Kármán elliptic microplate incorporating the Casimir force has not been investigated thus far.

The rest of the paper is organized as follows. In Sections 2 and 3, we describe, respectively, the electromechanical and the reduced-order models for a von Kármán plate under the effect of the Coulomb and the Casimir forces. In Section 4, we briefly outline the technique used to solve the reduced-order system of equations. In Section 5, we present static pull-in parameters and fundamental frequencies of microplates and micromembranes predeformed by the Coulomb and the Casimir forces. Conclusions are summarized in Section 6.

2. Formulation of the initial-boundary-value problem

Referring to the geometry in Fig. 1, we consider an elliptic plate-like body of major semiaxis $a>0$ and minor semiaxis $0<b<a$, placed into the three-dimensional space region $\Omega\times(-h/2,h/2)$. The mid-surface Ω is described by confocal elliptic coordinates (x^1,x^2), that are related to rectangular Cartesian coordinates (z^1,z^2) by

$$\begin{cases} z^1 = a\Theta\cosh x^1\cos x^2, \\ z^2 = a\Theta\sinh x^1\sin x^2, \end{cases} \quad x^1\in[0,x_b^1], \quad x^2\in[0,2\pi), \tag{1}$$

where $\Theta^2=1-b^2/a^2$ and $x_b^1=\operatorname{arctanh}(b/a)$, see for example Ref. [51].

Let $\mathbf{v}$ and $\mathbf{T}$ be a vector field and a second-order tensor field in Ω, respectively. In elliptic coordinates, the physical dimensions of the covariant components v_i and T_{ij} equal, respectively, Length and Length^2 multiplied with physical dimensions of the corresponding fields. For example, the physical dimensions of the covariant components of the in-plane displacement field are Length^2, and the physical dimensions of the covariant

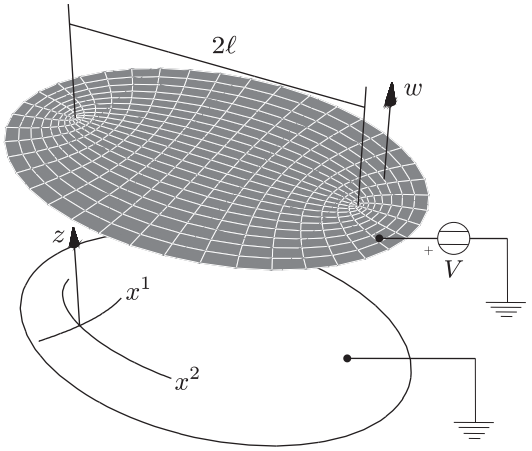

Fig. 1. Sketch of the electrostatically actuated device.

components of the in-plane stress field are force. In elliptic coordinates, the covariant, mixed, and contravariant components of the in-plane identity tensor are given by $a^2\Theta^2\chi\delta_{ij}$, δ^j_i, and $a^{-2}\Theta^{-2}\chi^{-1}\delta^{ij}$, respectively, where

$$\delta_{ij}=\delta^i_j=\delta^j_i=\delta^{ij}=\begin{cases}1 & \text{if } i=j,\\ 0 & \text{if } i\neq j\end{cases} \tag{2}$$

is the Kronecker delta, and the field χ is given by

$$\chi(x^1,x^2)=\tfrac{1}{2}(\cosh 2x^1-\cos 2x^2), \tag{3}$$

see for example Ref. [51].

We assume that the initial gap g_0 between the two conductors and the thickness h of the deformable plate are much smaller than the characteristic length a and that g_0 and h can be of the same order of magnitude. Therefore, the maximum displacement that the device can undergo is of the order of the plate thickness h, but it is much smaller than the characteristic length a, since $h/a\ll 1$. This implies that strains in the deformable electrode are small. Under these assumptions, we use the von Kármán plate theory to account for large deflections and small strains, see for example Ref. [50]. Neglecting the effect of the rotatory inertia, the von Kármán plate equations in elliptic coordinates are [50]

$$\varrho h\ddot{w}+\frac{D}{a^4\Theta^4\chi}\frac{\partial^2}{\partial x^k\partial x^k}\left(\frac{1}{\chi}\frac{\partial^2 w}{\partial x^j\partial x^j}\right)-\frac{h}{a^4\Theta^4\chi}\frac{\partial}{\partial x^j}\left(\frac{1}{\chi}\sigma_{jk}\frac{\partial w}{\partial x^k}\right)-F_e-F_c=0, \tag{4a}$$

$$\varrho\ddot{u}_i-\frac{1}{a^2\Theta^2\chi}\sigma_{ij\|j}=0,\quad i=1,2. \tag{4b}$$

We use the Einstein summation convention, meaning that when an index appears twice in a single term we sum over the range $\{1,2\}$ of the index; $\sigma_{ij\|k}$ is the covariant derivative of the covariant components σ_{ij} of the in-plane stress tensor field, that is,

$$\sigma_{ij\|k}=\frac{\partial\sigma_{ij}}{\partial x^k}-\left\{\begin{matrix}l\\ ik\end{matrix}\right\}\sigma_{lj}-\left\{\begin{matrix}l\\ jk\end{matrix}\right\}\sigma_{il} \tag{5}$$

with the fields $\{^{\,i}_{jk}\}$ defined by

$$\left\{\begin{matrix}i\\ jk\end{matrix}\right\}=\frac{1}{2\chi}\left(\delta^i_k\frac{\partial\chi}{\partial x^j}+\delta^i_j\frac{\partial\chi}{\partial x^k}-\delta^{il}\delta_{jk}\frac{\partial\chi}{\partial x^l}\right). \tag{6}$$

Furthermore in Eqs. (4), $D=Eh^3/(12(1-\nu^2))$ is the bending stiffness of the plate; ϱ, E, and ν are the mass density, the Young's modulus, and the Poisson's ratio of the plate material, that is assumed to be

homogeneous and isotropic; u_i and w are the in-plane and the out-of-plane displacements of a point on the mid-surface; F_e and F_c are the Coulomb and the Casimir forces; and a superimposed dot means time derivative. Expressions for the Coulomb and the Casimir forces are discussed below.

For a circular plate, $a = b$, and one needs to write Eqs. (4a) and (4b) in a different form.

We further note that when $\sigma_{ij} = \overline{\sigma} a^2 \Theta^2 \chi \delta_{ij}$, where $\overline{\sigma}$ is a scalar field having dimensions of stress, and the rigidity due to in-plane stretching dominates over the bending stiffness in supporting the external load, Eq. (4a) reduces to the equation governing the deformations of a linear elastic membrane.

In the von Kármán plate theory, the covariant components ε_{ij} of the in-plane strain tensor in elliptic coordinates are given by

$$\varepsilon_{ij} = \frac{1}{2}\left(u_{i\|j} + u_{j\|i} + \frac{\partial w}{\partial x^i}\frac{\partial w}{\partial x^j}\right), \tag{7}$$

where the covariant derivative of the in-plane displacement field is given by

$$u_{i\|j} = \frac{\partial u_i}{\partial x^j} - \begin{Bmatrix} k \\ ij \end{Bmatrix} u_k. \tag{8}$$

Assuming the response of the material to be linear elastic with the prestress $\overline{\sigma} a^2 \Theta^2 \chi \delta_{ij}$ in the reference configuration, the constitutive relation under the Kirchhoff assumption is, see for example Ref. [52],

$$\sigma_{ij} = \frac{E}{1+\nu}\left(\varepsilon_{ij} + \frac{\nu}{1-\nu}\varepsilon_{kk}\delta_{ij}\right) + \overline{\sigma} a^2 \Theta^2 \chi \delta_{ij}. \tag{9}$$

Substituting for σ_{ij} from Eq. (9) into Eq. (4), assuming that $\overline{\sigma}$ is a constant scalar field, and using Eq. (7), we obtain the following equations for u_i and w:

$$\begin{aligned} &\varrho h \ddot{w} + \frac{D}{a^4\Theta^4\chi}\frac{\partial^2}{\partial x^k \partial x^k}\left(\frac{1}{\chi}\frac{\partial^2 w}{\partial x^j \partial x^j}\right) - \frac{B}{a^4\Theta^4\chi}\frac{\partial}{\partial x^j}\left(\frac{1}{\chi}\left(\frac{1}{2}\left(u_{j\|k} + u_{k\|j}\right) + \frac{\partial u_l}{\partial x^l}\delta_{jk}\right)\frac{\partial w}{\partial x^k}\right) \\ &- \frac{B}{2a^4\Theta^4\chi}\frac{\partial}{\partial x^j}\left(\frac{1}{\chi}\frac{\partial w}{\partial x^l}\frac{\partial w}{\partial x^l}\frac{\partial w}{\partial x^j}\right) - \frac{\overline{\sigma} h}{a^2\Theta^2\chi}\frac{\partial^2 w}{\partial x^j \partial x^j} - F_e - F_c = 0, \end{aligned} \tag{10a}$$

$$\varrho h \ddot{u}_i - \frac{B}{2a^2\Theta^2}\left(\frac{1-\nu}{\chi}u_{i\|kk} + (1+\nu)\frac{\partial}{\partial x^i}\left(\frac{1}{\chi}\frac{\partial u_k}{\partial x^k}\right)\right) = \frac{B}{2a^2\Theta^2}\left((1-\nu)\frac{1}{\chi}\left(\frac{\partial w}{\partial x^i}\frac{\partial w}{\partial x^k}\right)_{\|k} + \nu\frac{\partial}{\partial x^i}\left(\frac{1}{\chi}\frac{\partial w}{\partial x^k}\frac{\partial w}{\partial x^k}\right)\right), \tag{10b}$$

where $B = Eh/(1-\nu^2)$ is the stretching stiffness of the plate.

From an electrical point of view, the system behaves as a variable gap capacitor. We do not consider fringing fields in the present work. By assuming that $g_0/a \ll 1$, the magnitude F_e of the electrostatic force acting on the deformable electrode along its normal is given by, see for example Refs. [5,53],

$$F_e = -\frac{\epsilon_0 V^2}{2g_0^2(1+\hat{w})^2}, \tag{11}$$

where $\hat{w} = w/g_0$ is the non-dimensional transverse displacement, and ϵ_0 is the dielectric constant in vacuum. Therefore, the expression for the electrostatic force at a point on the plate depends only on the local gap g. Thus, the validity of the analysis is limited to those variable gap capacitors whose actual gap is differentially uniform, that is, the two conductors are locally parallel to each other, see for example Refs. [5,53].

We use the proximity force approximation for the Casimir force F_c, that is consistent with assumptions made in the mechanical and the electrostatic models. In the proximity force approximation, curved surfaces are viewed as a superposition of infinitesimally small parallel plates, see for example Refs. [54,55] and references therein. In Ref. [55], it is shown that for a sphere of radius R separated from a flat plate by a distance g, the proximity force approximation gives results within 1% accuracy for $g/R < 0.1$. By adopting this

approximation we have

$$F_c = -\frac{\hbar c \pi^2}{240 g_0^4 (1+\hat{w})^4}, \tag{12}$$

where $\hbar$ is Plank's constant and c the speed of light in vacuum. Corrections to Eq. (12) for geometries with known and fixed departures from the parallel configurations are given in Refs. [54,55]. However, Eq. (12) is consistent with the parallel-plate approximation for the electrostatic force and with the small deformations assumption in the mechanical model. Both the Coulomb force and the Casimir force are assumed to act along the normal to the undeformed plate. Thus effects of changes in their orientations due to plate's deformations have been neglected.

For convenience, we introduce the non-dimensional time $\hat{t} = t/\tau$, where the characteristic time is defined by

$$\tau^2 = \frac{12\varrho a^4 \Theta^4}{Eh^2}(1-\nu^2) \tag{13}$$

and the non-dimensional in-plane displacement components $\hat{u}_i = u_i/g_0^2$, with $i = 1,2$. Henceforth, we use a superimposed dot to denote time derivative with respect to $\hat{t}$. Also, we drop the superimposed hat on non-dimensional variables. Thus, Eqs. (10) become

$$\ddot{w} + \frac{1}{\chi}\frac{\partial^2}{\partial x^k \partial x^k}\left(\frac{1}{\chi}\frac{\partial^2 w}{\partial x^j \partial x^j}\right) - \frac{12\alpha}{\chi}\frac{\partial}{\partial x^j}\left(\frac{1}{\chi}\left(\frac{1}{2}\left(u_{j\|k} + u_{k\|j}\right) + \frac{\partial u_l}{\partial x^l}\delta_{jk}\right)\frac{\partial w}{\partial x^k}\right)$$
$$- \frac{6\alpha}{\chi}\frac{\partial}{\partial x^j}\left(\frac{1}{\chi}\frac{\partial w}{\partial x^l}\frac{\partial w}{\partial x^l}\frac{\partial w}{\partial x^j}\right) - \frac{\beta}{\chi}\frac{\partial^2 w}{\partial x^j \partial x^j} + \frac{\lambda}{(1+w)^2} + \frac{\mu}{(1+w)^4} = 0, \tag{14a}$$

$$\gamma \ddot{u}_i - (1-\nu)\frac{u_{i\|kk}}{\chi} - (1+\nu)\frac{\partial}{\partial x^i}\left(\frac{1}{\chi}\frac{\partial u_k}{\partial x^k}\right) = (1-\nu)\frac{1}{\chi}\left(\frac{\partial w}{\partial x^i}\frac{\partial w}{\partial x^k}\right)_{\|k} + \nu\frac{\partial}{\partial x^i}\left(\frac{1}{\chi}\frac{\partial w}{\partial x^k}\frac{\partial w}{\partial x^k}\right), \tag{14b}$$

where

$$\alpha = \frac{g_0^2}{h^2}, \quad \beta = 12\frac{\overline{\sigma} a^2 \Theta^2}{Eh^2}(1-\nu^2), \quad \gamma = \frac{h^2}{6a^2\Theta^2},$$
$$\lambda = \frac{6\varepsilon_0 V^2 a^4 \Theta^4}{Eh^3 g_0^3}(1-\nu^2), \quad \mu = \frac{\hbar c \pi^2 a^4 \Theta^4}{20 Eh^3 g_0^5}(1-\nu^2). \tag{15}$$

Non-dimensional parameters β, λ, and μ are indicators of the MEMS relative stiffening due to the initial stress, the Coulomb force, and the Casimir force, respectively. Their values depend upon the elastic moduli of the material of the plate, the initial gap g_0, the plate thickness, and its geometry. With values of all other parameters kept fixed, a decrease in the initial gap g_0 increases μ significantly more than it increases λ. Since the von Kármán approximation holds for $h/a \ll 1$, we neglect in-plane the inertial term in Eq. (14b) and obtain the following simplified form for the in-plane motion:

$$(1-\nu)\frac{1}{\chi}u_{i\|kk} + (1+\nu)\frac{\partial}{\partial x^i}\left(\frac{1}{\chi}\frac{\partial u_k}{\partial x^k}\right) = -(1-\nu)\frac{1}{\chi}\left(\frac{\partial w}{\partial x^i}\frac{\partial w}{\partial x^k}\right)_{\|k} - \nu\frac{\partial}{\partial x^i}\left(\frac{1}{\chi}\frac{\partial w}{\partial x^k}\frac{\partial w}{\partial x^k}\right). \tag{16}$$

We note that Eq. (16) links the in-plane and the transverse displacements.

We consider the boundary Γ of Ω to be clamped. The kinematic boundary conditions for a clamped edge are [56]

$$w = 0 \quad \text{and} \quad \frac{\partial w}{\partial x^1} = 0, \tag{17a}$$

$$u_i = 0, \quad i = 1,2. \tag{17b}$$

Initial conditions are not needed since we either study static deformations of the MEMS or analyze resonance frequencies of small vibrations around an electrostatically deformed configuration.

3. Reduced-order system

A closed-form solution of the initial-boundary-value problem defined by Eqs. (14a) and (16) and boundary conditions (17) cannot be found. An approximate solution is constructed by expressing the displacement fields u_i, with $i = 1, 2$, and w through

$$w(x^1, x^2, t) = \sum_{n=1}^{N} \overline{w}_{(n)}(x^1, x^2)\zeta_{(n)}(t) = \mathbf{W}^{\mathrm{T}}(x^1, x^2)\boldsymbol{\zeta}(t), \tag{18a}$$

$$u_i(x^1, x^2, t) = \sum_{p=1}^{P} \overline{u}_{(p)i}(x^1, x^2)\xi_{(p)}(t) = \mathbf{U}^{\mathrm{T}}(x^1, x^2)\boldsymbol{\xi}(t), \tag{18b}$$

where $\overline{w}_{(n)}$ and $\overline{u}_{(p)i}$ are basis functions for the transverse and the in-plane displacements, and $\zeta_{(n)}$ and $\xi_{(p)}$ are the corresponding amplitude parameters or equivalently the mode participation factors. Basis functions are collected into the N-vector $\mathbf{W}$ and into the P-vector $\mathbf{U}$, and amplitudes are collected into the N-vector $\boldsymbol{\zeta}$ and into the P-vector $\boldsymbol{\xi}$. Each basis function satisfies the corresponding kinematic boundary conditions in Eqs. (17a) and (17b).

3.1. Basis functions for the in-plane displacement

A basis function for the in-plane displacement is determined by solving the following linear eigenvalue problem associated with Eq. (14b), see for example Ref. [50],

$$\kappa^2\overline{u}_i + (1-\nu)\frac{\overline{u}_{i\|kk}}{\chi} + (1+\nu)\frac{\partial}{\partial x^i}\left(\frac{1}{\chi}\frac{\partial u_k}{\partial x^k}\right) = 0, \tag{19}$$

where κ is the wave number. Following Ref. [50], we decompose the in-plane displacement as $\bar{u}_i = \bar{u}_i^n + \bar{u}_i^t$, $i = 1, 2$, where $\bar{u}_i^n$ and $\bar{u}_i^t$ are displacements associated, respectively, with the longitudinal and the transverse waves, and satisfy

$$e_3^{jk}\frac{\partial \overline{u}_j^n}{\partial x^k} = 0, \tag{20a}$$

$$\frac{\partial \overline{u}_k^t}{\partial x^k} = 0, \tag{20b}$$

where $e_i^{jk} = 0$ if any of the two indices are equal, and $e_i^{jk} = \pm 1$ if $\{i, j, k\}$ is an even or an odd permutation of $\{1, 2, 3\}$. Therefore, Eq. (19) is equivalent to the following two equations [50]:

$$\overline{u}_{i\|kk}^n + \chi\eta_n^2\overline{u}_i^n = 0, \tag{21a}$$

$$\overline{u}_{i\|kk}^t + \chi\eta_t^2\overline{u}_i^t = 0, \tag{21b}$$

where $\eta_n = \kappa/\sqrt{2}$ and $\eta_t = \kappa/\sqrt{1-\nu}$ are the wavenumbers of the longitudinal and the transverse waves, respectively.

Using Eq. (20a), we solve Eq. (21a) by introducing the scalar potential ϕ through $\overline{u}_i^n = \partial\phi/\partial x^i$. Therefore, within an arbitrary additive constant, Eq. (21a) reduces to

$$\frac{\partial^2\phi}{\partial x^j \partial x^j} + 2\hat{\eta}_n^2(\cosh 2x^1 - \cos 2x^2)\phi = 0, \tag{22}$$

where $2\hat{\eta}_n = \eta_n$.

In order to solve Eq. (21b), we use Eq. (20b) to introduce the vector potential Φ_j, $j = 1, 2, 3$, through $u_i^t = -e_i^{jk}\partial\phi_j/\partial x^k$. Since u_i^t are components of an in-plane vector field in Ω, we have that $\partial\Phi_1/\partial x^2 = \partial\Phi_2/\partial x^1$. Moreover, since the components of the vector potential are also in-plane fields in Ω, we have $\partial\Phi_1/\partial z = \partial\Phi_2/\partial z = 0$. It follows that, by defining the scalar field $\Phi = \Phi_3$, we can write $u_i^t = -e_i^{3k}\partial\Phi/\partial x^k$. Therefore, within an arbitrary additive vector field satisfying Eq. (20b), the vector eigenvalue problem defined

by Eq. (21b) reduces to the scalar one

$$\frac{\partial^2 \Phi}{\partial x^j \partial x^j} + 2\hat{\eta}_t^2(\cosh 2x^1 - \cos\, 2x^2)\Phi = 0, \tag{23}$$

where $2\hat{\eta}_t = \eta_t$.

By integrating Eq. (20) over the domain Ω and by applying the curl and the divergence theorems to transform surface integrals into line integrals, Eq. (20) implies the following set of boundary conditions for the displacements associated with the longitudinal and the transverse waves

$$\overline{u}_2^n(x_b^1, x^2) = 0, \quad \overline{u}_1^t(x_b^1, x^2) = 0. \tag{24}$$

Additional boundary conditions provided by Eq. (17b) are:

$$\overline{u}_1^n(x_b^1, x^2) = \overline{u}_2^t(x_b^1, x^2) = 0, \quad \overline{u}_2^t(x_b^1, x^2) = \overline{u}_1^n(x_b^1, x^2) = 0. \tag{25}$$

We note that the governing equations for the potentials ϕ and Φ, that is, Eqs. (22) and (23), respectively, are equivalent. Nevertheless, the normal and transverse displacement fields are generally different since the relation between them and their corresponding potentials are different. The general solution of Eqs. (22) and (23) is [57]

$$\psi(x^1, x^2) = \sum_{m=0}^{\infty} A_m^C \mathrm{Ce}_m(x^1, q)\mathrm{ce}_m(x^2, q) + \sum_{r=1}^{\infty} A_r^S \mathrm{Se}_r(x^1, q)\mathrm{se}_r(x^2, q), \tag{26}$$

where A_m^C and A_r^S are real constants, $\mathrm{Ce}_m(\eta, q) = \mathrm{ce}_m(\imath\eta, q)$, $\mathrm{Se}_r(\eta, q) = \mathrm{se}_r(\imath\eta, q)$, $\imath = \sqrt{-1}$, ce_m and se_r are the Mathieu cosine and the Mathieu sine functions of integer order. The characteristic parameter q equals $\hat{\eta}_n^2/4$ and $\hat{\eta}_t^2/4$ for normal and for transverse waves, respectively. Functions $\overline{u}_i^n$ and $\overline{u}_i^t$ are given by

$$\begin{aligned}
\overline{u}_1^n &= \frac{\partial \psi}{\partial x^1} \\
&= \sum_{m=0}^{\infty} A_m^C \frac{\partial \mathrm{Ce}_m}{\partial x^1}(x^1, q)\mathrm{ce}_m(x^2, q) + \sum_{r=1}^{\infty} A_r^S \frac{\partial \mathrm{Se}_r}{\partial x^1}(x^1, q)\mathrm{se}_r(x^2, q), \qquad (27a)\\
\overline{u}_2^n &= \frac{\partial \psi}{\partial x^2} \\
&= \sum_{m=0}^{\infty} A_m^C \mathrm{Ce}_m(x^1, q)\frac{\partial \mathrm{ce}_m}{\partial x^2}(x^2, q) + \sum_{r=1}^{\infty} A_r^S \mathrm{Se}_r(x^1, q)\frac{\partial \mathrm{se}_r}{\partial x^2}(x^2, q), \qquad (27b)\\
\overline{u}_1^t &= -\frac{\partial \psi}{\partial x^2}, \quad \overline{u}_2^t = \frac{\partial \psi}{\partial x^1}. \qquad (27c)
\end{aligned}$$

By imposing boundary conditions (24) and (25) on different families of independent functions, we find the characteristic equations

$$\frac{\partial \mathrm{Ce}_m}{\partial x^1}(x_b^1, \hat{p}) = 0, \quad \mathrm{Ce}_m(x_b^1, p) = 0, \tag{28a}$$

$$\frac{\partial \mathrm{Se}_r}{\partial x^1}(x_b^1, \hat{q}) = 0, \quad \mathrm{Se}_r(x_b^1, q) = 0. \tag{28b}$$

The roots of the characteristic equations (28) have been found with a computer code written in Mathematica using the built in functions `MathieuC` and `MathieuS`. The components of basis functions for the in-plane displacement are, therefore, given by the following families of functions:

$$\overline{u}_{(a_1)i}(x^1, x^2) = A_{mn}^1 \frac{\partial \mathrm{Ce}_m}{\partial x^1}(x^1, \hat{p}_{mn})\mathrm{ce}_m(x^2, \hat{p}_{mn}), \tag{29a}$$

$$\overline{u}_{(\overline{q}(\overline{p}+1)+a_2)i}(x^1, x^2) = A_{mn}^2 \mathrm{Ce}_m(x^1, p_{mn})\frac{\partial \mathrm{ce}_m}{\partial x^2}(x^2, p_{mn}), \tag{29b}$$

$$\overline{u}_{(2\overline{q}(\overline{p}+1)+a_3)i}(x^1, x^2) = A_{rn}^3 \frac{\partial \mathrm{Se}_r}{\partial x^1}(x^1, \hat{q}_{rn})\mathrm{se}_r(x^2, \hat{q}_{rn}), \tag{29c}$$

$$\overline{u}_{(\overline{q}(3\overline{p}+2)+a_4)i}(x^1,x^2)=A^4_{rn}\mathrm{Se}_r(x^1,q_{rn})\frac{\partial \mathrm{se}_r}{\partial x^2}(x^2,q_{rn}),\quad i=1,2, \tag{29d}$$

where

$$a_1=a_2=m\overline{q}+n,\quad a_3=a_4=(r-1)\overline{q}+n,$$
$$m=0,\ldots,\overline{p},\quad r=1,\ldots,\overline{p},\quad n=1,\ldots,\overline{q}. \tag{30}$$

The characteristic values $\hat{p}_{mn}$, p_{mn}, $\hat{q}_{rn}$, and q_{rn} are the nth roots of the characteristic Eqs. (28). The number of basis functions for the in-plane displacement in Eq. (18b) is $P=2\overline{q}(1+2\overline{p})$.

3.2. Basis functions for the transverse displacement

As basis functions for the transverse displacement we use the following family of functions:

$$\overline{w}_{(n)}(x^1,x^2)=A_n\left(\frac{\mathrm{Ce}_0(x^1,r_n)}{\mathrm{Ce}_0(x^1_b,r_n)}-\frac{\mathrm{Ce}_0(x^1,-r_n)}{\mathrm{Ce}_0(x^1_b,-r_n)}\right)\mathrm{ce}_0(x^2,r_n),\quad n=1,\ldots,N, \tag{31}$$

where A_n is a constant, and the characteristic values r_n are determined as roots of the transcendental equation

$$\frac{\partial \mathrm{Ce}_0}{\partial x^1}(x^1_b,r)\mathrm{Ce}_0(x^1_b,-r)-\frac{\partial \mathrm{Ce}_0}{\partial x^1}(x^1_b,-r)\mathrm{Ce}_0(x^1_b,r)=0. \tag{32}$$

Basis functions in Eq. (31) satisfy boundary conditions (17a) and are symmetric with respect to both the major and the minor axes [57], thereby ruling out a solution (if there is one) that is asymmetric about either one of the two axes. The roots of the characteristic Eq. (32) have been found with a computer code written in Mathematica and based on the use of the built in function `MathieuC`.

3.3. Relation between $\boldsymbol{\xi}$ and $\boldsymbol{\zeta}$

In order to express $\boldsymbol{\xi}$ in terms of $\boldsymbol{\zeta}$, we substitute from Eqs. (18a) and (18b) into Eq. (16), take the inner product of both sides of the resulting equation with the in-plane mode $\overline{u}_{(p)i}$, and integrate over the domain Ω. Applying the divergence theorem and imposing boundary conditions (17b) on the boundary integrals we obtain

$$\xi_{(p)}=\boldsymbol{\zeta}^{\mathrm{T}}\mathbf{H}_{(p)}\boldsymbol{\zeta}, \tag{33}$$

where the $(N\times N)$ symmetric matrix $\mathbf{H}_{(p)}$ is given by

$$[\mathbf{H}_{(p)}]_{mn}=-\int_\Omega\frac{1}{\chi^2}\left((1-\nu)\overline{u}_{(p)j\|k}\frac{\partial\overline{w}_{(m)}}{\partial x^j}\frac{\partial\overline{w}_{(n)}}{\partial x^k}+\nu\frac{\partial\overline{u}_{(p)k}}{\partial x^k}\frac{\partial\overline{w}_{(m)}}{\partial x^j}\frac{\partial\overline{w}_{(n)}}{\partial x^j}\right)\mathrm{d}\Omega$$
$$\times\left(\int_\Omega\frac{1}{\chi^2}((1-\nu)\overline{u}_{(p)j\|k}\overline{u}_{(p)j\|k}+(1+\nu)(\overline{u}_{(p)k\|k})^2)\,\mathrm{d}\Omega\right)^{-1},\quad m,n=1,\ldots,N \tag{34}$$

The covariant derivative $\overline{u}_{(p)i\|j}$ is computed according to the formula given as Eq. (8).

We note that all amplitude coefficients for the transverse displacement are needed for computing any amplitude coefficient of the in-plane displacement field. In addition, we note that the relation between the in-plane motion and the transverse motion is nonlinear, and that the in-plane motion vanishes in the linear theory. Because of the P internal constraints (33), the reduced-order model for the microplate has N degrees of freedom.

3.4. Equations for the reduced-order system

The reduced-order model is obtained by premultiplying both sides of Eq. (14a) by $\mathbf{W}$, integrating the resulting equation over Ω, and substituting into it the approximations given by Eqs. (18) and (33).

Therefore, we obtain

$$\int_\Omega \mathbf{W}\mathbf{W}^{\mathrm{T}}\ddot{\boldsymbol{\zeta}}\,\mathrm{d}\Omega + \int_\Omega \mathbf{W}\frac{1}{\chi}\frac{\partial^2}{\partial x^k \partial x^k}\left(\frac{1}{\chi}\frac{\partial^2}{\partial x^j \partial x^j}(\mathbf{W}^{\mathrm{T}}\boldsymbol{\zeta})\right)\mathrm{d}\Omega - 12\alpha\int_\Omega \mathbf{W}\frac{1}{\chi}\frac{\partial}{\partial x^j}\left(\frac{1}{\chi}\overline{\varepsilon}_{jk}\frac{\partial}{\partial x^k}(\mathbf{W}^{\mathrm{T}}\boldsymbol{\zeta})\right)\mathrm{d}\Omega$$
$$- 6\alpha\int_\Omega \mathbf{W}\frac{1}{\chi}\frac{\partial}{\partial x^j}\left(\frac{1}{\chi}\frac{\partial(\mathbf{W}^{\mathrm{T}}\boldsymbol{\zeta})}{\partial x^k}\frac{\partial(\mathbf{W}^{\mathrm{T}}\boldsymbol{\zeta})}{\partial x^k}\frac{\partial(\mathbf{W}^{\mathrm{T}}\boldsymbol{\zeta})}{\partial x^j}\right)\mathrm{d}\Omega - \beta\int_\Omega \mathbf{W}\frac{1}{\chi}\frac{\partial^2}{\partial x^j \partial x^j}(\mathbf{W}^{\mathrm{T}}\boldsymbol{\zeta})\,\mathrm{d}\Omega$$
$$+ \lambda\int_\Omega \frac{\mathbf{W}}{(1+\mathbf{W}^{\mathrm{T}}\boldsymbol{\zeta})^2}\,\mathrm{d}\Omega + \mu\int_\Omega \frac{\mathbf{W}}{(1+\mathbf{W}^{\mathrm{T}}\boldsymbol{\zeta})^4}\,\mathrm{d}\Omega = \mathbf{0}, \tag{35}$$

where

$$\overline{\varepsilon}_{ij} = \sum_{p=1}^{P}\xi_{(p)}(\boldsymbol{\zeta})V_{(p)ij} = \sum_{p=1}^{P}(\boldsymbol{\zeta}^{\mathrm{T}}\mathbf{H}_{(p)}\boldsymbol{\zeta})V_{(p)ij}, \tag{36a}$$

$$V_{(p)ij} = \frac{(1-\nu)}{2}(\overline{u}_{(p)i\|j} + \overline{u}_{(p)j\|i}) + \nu\left(\frac{\partial\overline{u}_{(p)k}}{\partial x^k}\right)\delta_{ij}. \tag{36b}$$

From Eqs. (34) and (36), we note that the normalization constants introduced in Eq. (29) do not affect $\overline{\varepsilon}_{ij}$. We now define the following $(N \times N)$ matrices:

$$[\mathbf{D}]_{mn} = \frac{1}{\chi}\frac{\partial\overline{w}_{(m)}}{\partial x^j}\frac{\partial\overline{w}_{(n)}}{\partial x^j}, \tag{37a}$$

$$[\mathbf{L}]_{mn} = \frac{1}{\chi^2}\frac{\partial^2\overline{w}_{(m)}}{\partial x^j \partial x^j}\frac{\partial^2\overline{w}_{(n)}}{\partial x^k \partial x^k}, \tag{37b}$$

$$[\mathbf{G}]_{mn} = \frac{\overline{\varepsilon}_{jk}}{\chi^2}\frac{\partial\overline{w}_{(m)}}{\partial x^j}\frac{\partial\overline{w}_{(n)}}{\partial x^k} \tag{37c}$$

with $m,n = 1,\ldots,N$. Using the divergence theorem and imposing the boundary conditions in Eq. (17a), we obtain the following equation for the reduced-order system:

$$\mathbf{m}\ddot{\boldsymbol{\zeta}} + (\mathbf{k}_1 + \beta\mathbf{k}_2 + \alpha\mathbf{k}_3(\boldsymbol{\zeta}))\boldsymbol{\zeta} + \lambda\mathbf{f}_e(\boldsymbol{\zeta}) + \mu\mathbf{f}_c(\boldsymbol{\zeta}) = \mathbf{0}, \tag{38}$$

where

$$\mathbf{m} = \int_\Omega \mathbf{W}\mathbf{W}^{\mathrm{T}}\,\mathrm{d}\Omega, \tag{39a}$$

$$\mathbf{k}_1 = \int_\Omega \mathbf{L}\,\mathrm{d}\Omega, \quad \mathbf{k}_2 = \int_\Omega \mathbf{D}\,\mathrm{d}\Omega, \tag{39b}$$

$$\mathbf{k}_3(\boldsymbol{\zeta}) = 12\int_\Omega\left(\mathbf{G} + \frac{1}{2}(\boldsymbol{\zeta}^{\mathrm{T}}\mathbf{D}\boldsymbol{\zeta})\mathbf{D}\right)\mathrm{d}\Omega, \tag{39c}$$

$$\mathbf{f}_e(\boldsymbol{\zeta}) = \int_\Omega \frac{\mathbf{W}}{(1+\mathbf{W}^{\mathrm{T}}\boldsymbol{\zeta})^2}\,\mathrm{d}\Omega, \quad \mathbf{f}_c(\boldsymbol{\zeta}) = \int_\Omega \frac{\mathbf{W}}{(1+\mathbf{W}^{\mathrm{T}}\boldsymbol{\zeta})^4}\,\mathrm{d}\Omega. \tag{39d}$$

In Eq. (38), $(\mathbf{k}_1 + \beta\mathbf{k}_2)$ represents the stiffness of a linear elastic plate, and $\alpha\mathbf{k}_3(\boldsymbol{\zeta})$ represents the strain-stiffening effect.

We note that the system represented by Eq. (38) depends on N displacement unknowns. As shown below, $N = 1$ gives very good results.

4. Static pull-in parameters

The tangent stiffness matrix of the reduced-order system is given by

$$\mathbf{K}(\boldsymbol{\zeta},\lambda,\mu)=\mathbf{k}_1+\beta\mathbf{k}_2+\alpha\mathbf{k}_3(\boldsymbol{\zeta})+\alpha\frac{\mathrm{d}\mathbf{k}_3(\boldsymbol{\zeta})}{\mathrm{d}\boldsymbol{\zeta}}\boldsymbol{\zeta}+\lambda\frac{\mathrm{d}\mathbf{f}_e(\boldsymbol{\zeta})}{\mathrm{d}\boldsymbol{\zeta}}+\mu\frac{\mathrm{d}\mathbf{f}_c(\boldsymbol{\zeta})}{\mathrm{d}\boldsymbol{\zeta}}, \tag{40}$$

where

$$\frac{\mathrm{d}\mathbf{f}_e(\boldsymbol{\zeta})}{\mathrm{d}\boldsymbol{\zeta}}=-2\int_\Omega\frac{\mathbf{W}\mathbf{W}^{\mathrm{T}}}{(1+\mathbf{W}^{\mathrm{T}}\boldsymbol{\zeta})^3}\,\mathrm{d}\Omega,\quad \frac{\mathrm{d}\mathbf{f}_c(\boldsymbol{\zeta})}{\mathrm{d}\boldsymbol{\zeta}}=-4\int_\Omega\frac{\mathbf{W}\mathbf{W}^{\mathrm{T}}}{(1+\mathbf{W}^{\mathrm{T}}\boldsymbol{\zeta})^5}\,\mathrm{d}\Omega. \tag{41}$$

From Eqs. (36a) and (37c), we obtain

$$\frac{\mathrm{d}[\mathbf{G}]_{mn}}{\mathrm{d}\boldsymbol{\zeta}}\boldsymbol{\zeta}=\left[2\sum_{p=1}^{P}\left(\frac{1}{\chi^2}V_{(p)jk}\frac{\partial\overline{w}_{(m)}}{\partial x^j}\frac{\partial\overline{w}_{(n)}}{\partial x^k}\right)\boldsymbol{\zeta}^{\mathrm{T}}\mathbf{H}_{(p)}\right]\boldsymbol{\zeta}=2[\mathbf{G}]_{mn}, \tag{42}$$

and similarly

$$\frac{\mathrm{d}(\boldsymbol{\zeta}^{\mathrm{T}}\mathbf{D}\boldsymbol{\zeta})[\mathbf{D}]_{mn}}{\mathrm{d}\boldsymbol{\zeta}}\boldsymbol{\zeta}=2(\boldsymbol{\zeta}^{\mathrm{T}}\mathbf{D}\boldsymbol{\zeta})[\mathbf{D}]_{mn}. \tag{43}$$

Differentiating both sides of Eq. (39c) with respect to $\boldsymbol{\zeta}$, and substituting from Eqs. (42) and (43) into the result, we get

$$\frac{\mathrm{d}\mathbf{k}_3(\boldsymbol{\zeta})}{\mathrm{d}\boldsymbol{\zeta}}\boldsymbol{\zeta}=2\mathbf{k}_3(\boldsymbol{\zeta}). \tag{44}$$

Therefore, Eq. (40) can be rewritten as

$$\mathbf{K}(\boldsymbol{\zeta},\lambda,\mu)=\mathbf{k}_1+\beta\mathbf{k}_2+3\alpha\mathbf{k}_3(\boldsymbol{\zeta})+\lambda\frac{\mathrm{d}\mathbf{f}_e(\boldsymbol{\zeta})}{\mathrm{d}\boldsymbol{\zeta}}+\mu\frac{\mathrm{d}\mathbf{f}_c(\boldsymbol{\zeta})}{\mathrm{d}\boldsymbol{\zeta}}. \tag{45}$$

In what follows, we discuss two equivalent methods to extract static pull-in parameters. The first one is based on the solution of the static problem, while the second one is based on the study of small vibrations of the system around static equilibria. The method based on frequency analysis can be used to experimentally determine the pull-in voltage [9].

4.1. Extraction of pull-in parameters from the static problem

At the onset of instability the system's tangent stiffness matrix becomes singular. Therefore, at pull-in the system satisfies Eq. (38) with $\ddot{\boldsymbol{\zeta}}=\mathbf{0}$ and the additional condition

$$\det\mathbf{K}(\boldsymbol{\zeta},\lambda,\mu)=0. \tag{46}$$

Critical value of μ: The static problem is solved for $\lambda=0$ to compute the critical value, μ_{cr}, of the Casimir force parameter. When $\mu=\mu_{\mathrm{cr}}$ the system collapses spontaneously without applying any voltage, that is, with $V=0$. Thus, such a MEMS can not be fabricated.

Pull-in parameters: The effect of the MEMS size on pull-in parameters λ_{PI} and $\|w_{\mathrm{PI}}\|_\infty$ is investigated by solving Eq. (38) with variable λ for different values of μ in the range $[0,\mu_{\mathrm{cr}}]$. The pull-in instability $(\lambda_{\mathrm{PI}},\|w_{\mathrm{PI}}\|_\infty)$ occurs when the curve $\|w\|_\infty(\lambda,\mu)$ becomes multi-valued. Here $\|\cdot\|_\infty$ is defined as $\max_{(x^1,x^2)\in\Omega}|\cdot|$.

We use the displacement iteration pull-in extraction (DIPIE) algorithm [58] to solve Eq. (38) with $\ddot{\boldsymbol{\zeta}}=\mathbf{0}$. This algorithm enables one to find the complete bifurcation path by driving the system through the displacement of a pre-chosen point $(\overline{x}^1,\overline{x}^2)\in\Omega$ and by treating the load parameter (either λ or μ) as unknown. The method is explained for the case of variable λ and fixed μ. When studying the behavior of the system under the effect of the Casimir force only, that is, for $\lambda=0$ with varying μ, exactly the same procedure applies except that the roles of the two parameters are reversed.

A parameter s, representing the deflection of a point $(\overline{x}^1,\overline{x}^2)\in\Omega$, is added. Both $\boldsymbol{\zeta}$ and λ are regarded as functions of s. If the solution $(\boldsymbol{\zeta}_{i-1},\lambda_{i-1})$ of Eqs. (38) and (46) at the $(i-1)$th load step $s_{i-1}=\mathbf{W}^{\mathrm{T}}(\overline{x}^1,\overline{x}^2)\boldsymbol{\zeta}_{i-1}$ is

known, then the solution $(\zeta_i, \lambda_i) = (\zeta_{i-1}, \lambda_{i-1}) + (\Delta\zeta_i, \Delta\lambda_i)$ corresponding to $s_i = s_{i-1} + \Delta s_i$ is obtained by solving the following system of equations:

$$(\mathbf{k}_1 + \beta\mathbf{k}_2 + \alpha\mathbf{k}_3(\zeta_i))\zeta_i + \lambda_i\mathbf{f}_e(\zeta_i) + \mu\mathbf{f}_c(\zeta_i) = \mathbf{0}, \tag{47a}$$

$$\mathbf{W}^{\mathrm{T}}(\overline{x}^1, \overline{x}^2)\zeta_i = s_i. \tag{47b}$$

The index i here refers to the ith load step rather than to the component of a field along the x^i coordinate. The solution of the set of nonlinear Eqs. (47) in terms of the unknowns $\Delta\zeta_i$ and $\Delta\lambda_i$ is found by using Newton's iterations. Hence, at the generic jth iteration, we have

$$\begin{bmatrix} \mathbf{K}(\zeta_i^{(j)}, \lambda_i^{(j)}, \mu) & \frac{\mathrm{d}\mathbf{f}_e(\zeta_i^{(j)})}{\mathrm{d}\zeta} \\ \mathbf{W}^{\mathrm{T}}(\overline{x}^1, \overline{x}^2) & 0 \end{bmatrix} \begin{bmatrix} \Delta\zeta_i^{(j)} \\ \Delta\lambda_i^{(j)} \end{bmatrix} = - \begin{bmatrix} (\mathbf{k}_1 + \beta\mathbf{k}_2 + \alpha\mathbf{k}_3(\zeta_i^{(j)}))\zeta_i^{(j)} + \lambda_i^{(j)}\mathbf{f}_e(\zeta_i^{(j)}) + \mu\mathbf{f}_c(\zeta_i^{(j)}) \\ \mathbf{W}^{\mathrm{T}}(\overline{x}^1, \overline{x}^2)\zeta_i^{(j)} - s_i \end{bmatrix}, \tag{48}$$

where $(\Delta\zeta_i^{(j)}, \Delta\lambda_i^{(j)})$ indicates the jth solution increment, and $(\zeta_i^{(j)}, \lambda_i^{(j)})$ is the updated solution at the $(j-1)$th iteration. That is,

$$\zeta_i^{(j)} = \zeta_{i-1} + \sum_{k=1}^{j-1} \Delta\zeta_i^{(k)}, \quad \lambda_i^{(j)} = \lambda_{i-1} + \sum_{k=1}^{j-1} \Delta\lambda_i^{(k)}. \tag{49}$$

The iterations are performed until

$$\max[|\Delta\zeta_i^{(j)}|, \Delta\lambda_i^{(j)}] \leqslant \varepsilon_T, \tag{50}$$

where ε_T is a preassigned small number.

The pull-in value of λ equals the maximum value of λ for which Eqs. (47) have a solution.

4.2. Extraction of pull-in parameters from the linear eigenvalue problem

The natural frequencies, ω, of the deflected plate at a given converged solution $(\zeta_i, \lambda_i, \mu_i)$ up to pull-in are found as follows. We set $\lambda = \lambda_i$ and $\mu = \mu_i$ in Eq. (38), and we perturb the equilibrium state ζ_i with a harmonic term $\exp(\imath\omega t)$ as $\zeta_i(t) + \underline{\zeta}_i \exp(\imath\omega t)$, where $\underline{\zeta}_i$ is a constant vector and $\|\underline{\zeta}_i\| \ll \|\zeta_i\|$. By retaining only terms linear in $\underline{\zeta}_i$ we obtain the following equation for the determination of ω:

$$\det(\mathbf{K}(\zeta_i, \lambda_i, \mu_i) - \omega^2\mathbf{m}) = 0. \tag{51}$$

Since the tangent stiffness matrix becomes singular at pull-in, it follows that at the pull-in at least one natural frequency of the system equals zero. This can be viewed as an alternative way of defining the static pull-in, see Refs. [6,9,23,24].

5. Results

We have developed a computer code, in Mathematica, to solve the system of nonlinear Eqs. (47) for the pull-in parameters and to compute the lowest eigenvalue from Eq. (51).

Integrals appearing in the reduced-order model for the microplate have been evaluated using the Gauss quadrature rule by placing 21×21 quadrature points in the region $[0, x_b^1] \times [0, 2\pi]$. It was found that the consideration of additional quadrature points did not improve the solution accuracy. A large number of integration points are needed since integrals are defined over the entire elliptical region.

Results presented below for clamped elliptic plates are for $\nu = 0.25$. We apply constant increments $|\Delta s_i| = 10^{-3}$ to extract pull-in parameters with the DIPIE algorithm. Tolerance ε_T in Eq. (50) equals 10^{-7}. For $\lambda = 0$ and $\mu = 0$, the numerical scheme is started with $s_0 = 0$, consistent with the assumption that the corresponding deflection of every point on the plate's mid-surface is zero. We impose the displacement s at the point $(\overline{x}^1, \overline{x}^2) = (0, \pi/2)$.

We solve the problem for $\lambda = 0$ to determine the critical parameters $(\zeta_{\mathrm{cr}}, \mu_{\mathrm{cr}})$, corresponding to the collapse of the system with zero applied voltage, that is only due to the Casimir force. When solving the problem with

variable λ and assigning values to μ in the range $[0, \mu_{cr}]$, the DIPIE scheme is started with $s_0 = \mathbf{W}^T(\overline{x}^1, \overline{x}^2)\boldsymbol{\zeta}_\mu$, where $\boldsymbol{\zeta}_\mu$ is the converged set of deflection parameters corresponding to $\lambda = 0$.

Results are computed with $\overline{q} = \overline{p}$ in Eq. (29). Thus the total number of basis functions used to approximate the displacement field equals $N + P = N + 2\overline{p}(1 + 2\overline{p})$, see Section 3; whereas the total number of degrees of freedom equals N.

5.1. Pull-in parameters from the analysis of the static problem

Tables 1 and 2 show the critical Casimir force parameters $\|w_{cr}\|_\infty$ and μ_{cr} extracted for $\alpha = 1$, $\beta = 0$, two aspect ratios b/a, and different values of $\overline{p}$, $\overline{q}$, and N in Eqs. (29) and (31). For the same number of basis functions for the in-plane displacement, solutions computed with $N = 1$ differ from those computed with $N = 5$ by only $\approxeq 1\%$.

According to values listed in Tables 1 and 2 we adopt $\overline{p} = \overline{q} = 2$ and $N = 1$ to compute results presented below. Thus the reduced-order system has 1 degree-of-freedom and 20 basis functions for the in-plane displacement.

For $\alpha = 1/(12(1 - \nu^2))$, $\beta = 0$, and $b/a = 0.99$, the converged pull-in parameters $\|w_{PI}\|_\infty = 0.470$ and $\lambda_{PI} = 14.4$ match well with the corresponding ones $\|w_{PI}\|_\infty \approxeq 0.47$ and $\lambda_{PI} \approxeq 14$ obtained from Fig. 2 of Ref. [24], wherein the reduced-order model for a circular von Kármán microplate has been formulated in terms of the transverse displacement and the Airy stress function. This validates our model and provides additional justification for taking $\overline{p} = \overline{q} = 2$ and $N = 1$.

In Fig. 2, we plot μ_{cr} versus b/a for $\alpha = 1$ and 4. Due to an increase in the stiffness of the system with a decrease in the aspect ratio b/a, the critical value of the Casimir force parameter increases significantly with a decrease in b/a. The critical Casimir force parameters data (points in Fig. 2) are fitted with a fourth order polynomial in a/b (solid lines in Fig. 2):

$$\mu_{cr} = f(\alpha)\left(1 + \left(\frac{a}{b}\right)^2 + \left(\frac{a}{b}\right)^4\right). \tag{52}$$

Table 1
For $b/a = 0.5$, the critical Casimir force parameter μ_{cr} and the corresponding pull-in displacement infinity norm $\|w_{cr}\|_\infty$ with different number of basis functions for the in-plane and the transverse displacements

N	$\|w_{cr}\|_\infty$			μ_{cr}		
	$\overline{p}, \overline{q} = \overline{p}$			$\overline{p}, \overline{q} = \overline{p}$		
	1	2	4	1	2	4
1	0.316	0.311	0.310	64.7	63.9	63.8
3	0.313	0.308	0.308	64.4	63.6	63.6
5	0.313	0.308	0.307	64.4	63.6	63.6

Table 2
For $b/a = 0.75$, the critical Casimir force parameter μ_{cr} and the corresponding pull-in displacement infinity norm $\|w_{cr}\|_\infty$ with different number of basis functions for the in-plane and the transverse displacements

N	$\|w_{cr}\|_\infty$			μ_{cr}		
	$\overline{p}, \overline{q} = \overline{p}$			$\overline{p}, \overline{q} = \overline{p}$		
	1	2	4	1	2	4
1	0.304	0.302	0.302	25.2	25.1	25.1
3	0.300	0.299	0.299	25.2	25.1	25.1
5	0.300	0.299	0.299	25.2	25.1	25.1

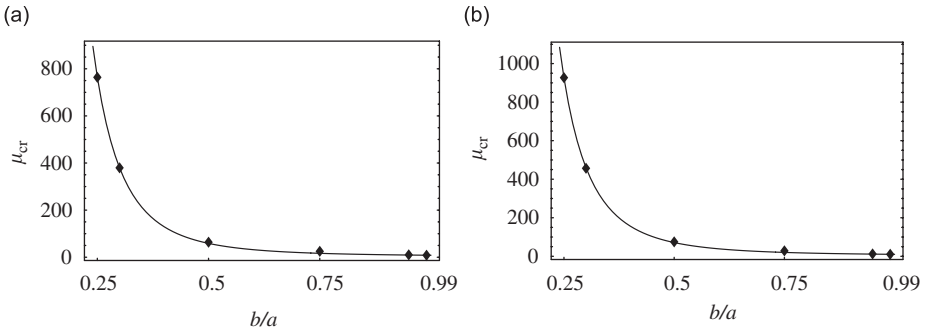

Fig. 2. Variation of μ_{cr} with the aspect ratio b/a for (a) $\alpha = 1$ and (b) $\alpha = 4$.

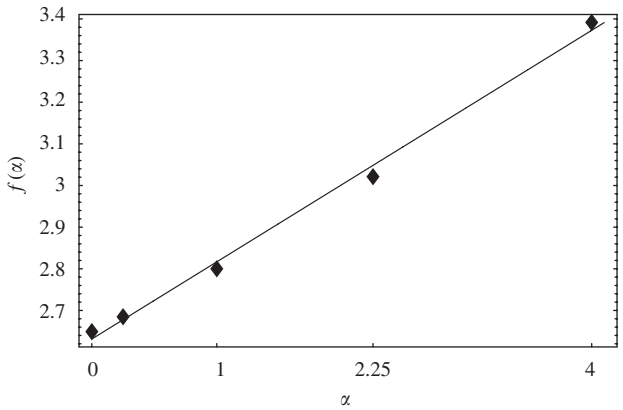

Fig. 3. Variation with α of the function $f(\alpha)$ in Eq. (52).

The function $f(\alpha)$ is plotted in Fig. 3 for $\alpha \in [0, 4]$ with the solid line corresponding to the function

$$f(\alpha) = 2.63 + 0.185\alpha. \tag{53}$$

Eq. (52) can be solved for a/b in terms of α and μ_{cr}. Among the four roots, the only one real and positive root is

$$\frac{a}{b} = \sqrt{\frac{\sqrt{1 - 4\varphi(\alpha, \mu_{cr})} - 1}{2}}, \tag{54}$$

for $\varphi(\alpha, \mu_{cr}) < 0$, where

$$\varphi(\alpha, \mu_{cr}) = 1 - \frac{\mu_{cr}}{f(\alpha)}. \tag{55}$$

Thus, since μ_{cr} is a monotonically increasing function of a/b, for a given α Eq. (54) yields the minimum ratio a/b of the elliptic MEMS that can be safely fabricated.

We note that μ_{cr} rapidly increases with an increase in a/b. Hence for the same value of g_0/h, a clamped elliptic plate with a large value of a/b is less likely to collapse during the fabrication process than a clamped circular plate with radius equal to a.

Pull-in parameters versus μ in the range $[0, \mu_{cr}]$ for $\alpha = 1$, $\beta = 0$, and two aspect ratios of the plate are plotted in Figs. 4 and 5. As μ increases, the pull-in parameter λ_{PI} decreases monotonically from its maximum value λ_{PI}^{max} corresponding to $\mu = 0$ to its minimum value 0 for $\mu = \mu_{cr}$; $\mu = \mu_{cr}$ represents the intersection of the curves with the horizontal axis. With an increase in μ the non-dimensional maximum transverse displacement decreases monotonically from its maximum value $\|w_{PI}\|_{\infty}^{max}$ for $\mu = 0$. This means that reduced deflection

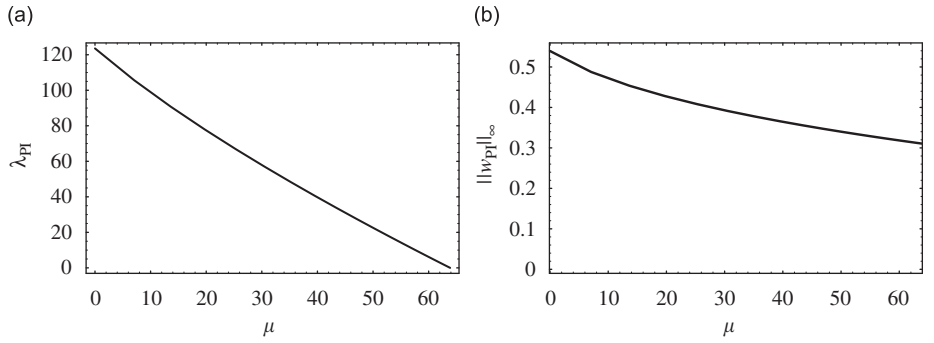

Fig. 4. For an elliptic plate with $\alpha = 1$, $\beta = 0$ and $b/a = 0.5$, the variation with μ of (a) λ_{PI} and (b) $\|w_{PI}\|_\infty$.

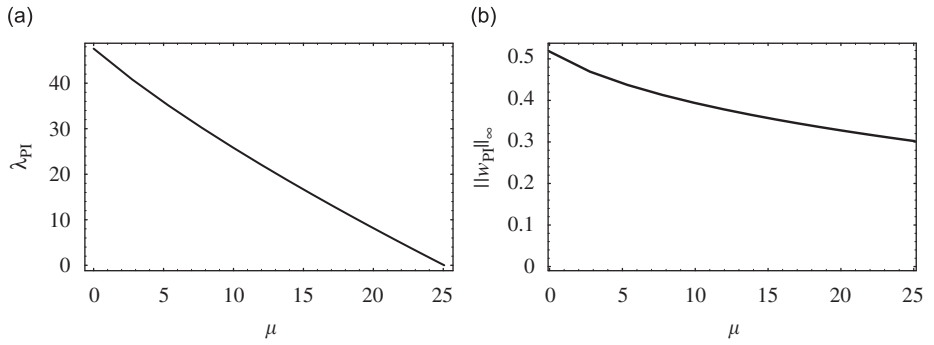

Fig. 5. For an elliptic plate with $\alpha = 1$, $\beta = 0$ and $b/a = 0.75$, the variation with μ of (a) λ_{PI} and (b) $\|w_{PI}\|_\infty$.

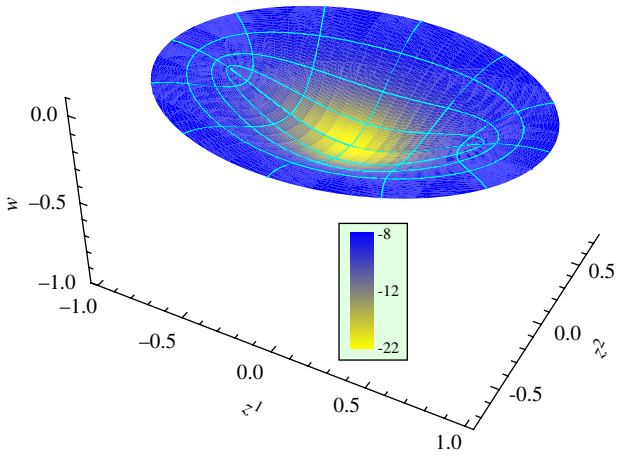

Fig. 6. Deformed shape of the elliptic plate with $b/a = 0.75$ for $\alpha = 1$, $\beta = 0$, $\mu \simeq 0.3\mu_{cr}$, $\lambda \simeq 30$, and $\|w\|_\infty \simeq 0.41$, and fringe plots of the Casimir pressure.

ranges are allowable for small devices. By comparing results depicted in Figs. 4 and 5, we conclude that a decrease in the aspect ratio of an elliptic plate from 0.75 to 0.5 significantly increases λ_{PI}^{max}, and it does not noticeably affect the difference $\|w_{PI}\|_\infty^{max} - \|w_{cr}\|_\infty$, where $\|w_{cr}\|_\infty$ is $\|w_{PI}\|_\infty$ corresponding to $\lambda = 0$.

Fig. 6 exhibits the deformed shape of the plate with $b/a = 0.75$ near pull-in for $\mu \simeq 0.3\mu_{cr}$, i.e., when $\lambda = \simeq 30$ and $\|w\|_\infty \simeq 0.41$. Fringe plots of the Casimir pressure given in Eq. (12) are also shown on the deformed shape of the plate. It is clear that boundary conditions in Eq. (17a) are well satisfied, and as

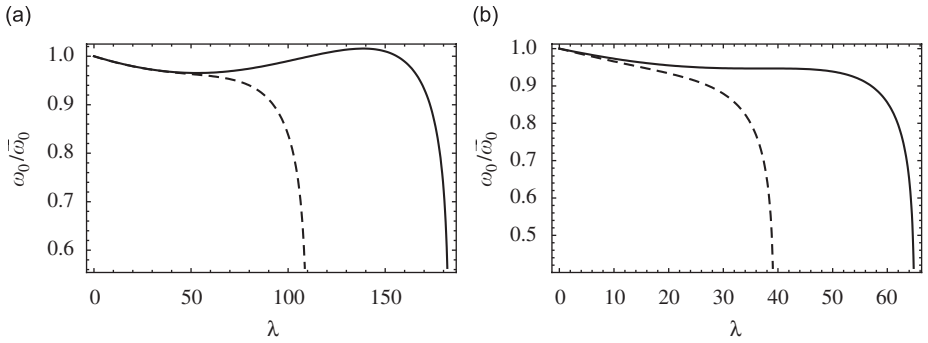

Fig. 7. Normalized fundamental natural frequency versus λ for $\mu = 0$ (solid line), $\mu \simeq 0.3\mu_{cr}$ (dashed line), and $\alpha = 4$, $\beta = 0$; (a) $b/a = 0.5$ and (b) $b/a = 0.75$.

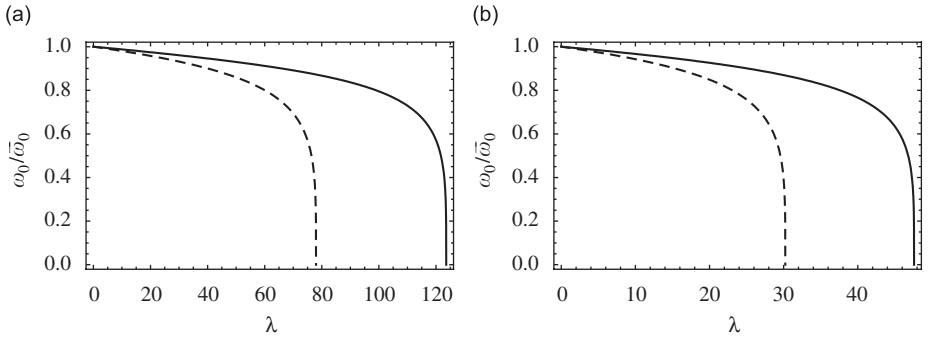

Fig. 8. Normalized fundamental natural frequency versus λ for $\mu = 0$ (solid line), $\mu \simeq 0.3\mu_{cr}$ (dashed line), and $\alpha = 1$, $\beta = 0$; (a) $b/a = 0.5$ and (b) $b/a = 0.75$.

expected, the absolute value of the Casimir pressure is maximum around the plate centroid and minimum at points near the supports.

5.2. *Pull-in parameters from the analysis of frequencies of a deformed plate*

In Fig. 7, we plot for two aspect ratios the fundamental natural frequency ω_0 of the deflected microplate versus λ for $\alpha = 4$, $\beta = 0$ (that is, no initial stress) and two different values of μ. The natural frequency is normalized with respect to the value $\overline{\omega}_0$ corresponding to $\lambda = 0$. The trend is non-monotonic due to the combined effect of the strain hardening represented by $\mathbf{k}_3(\boldsymbol{\zeta})$ and the softening effect introduced by the Coulomb and the Casimir forces. Indeed, from Eq. (41) it is clear that the overall effect of the Coulomb and the Casimir forces is equivalent to a nonlinear spring with negative tangent stiffness. When the overall strain-hardening effect is negligible, for example when $\mu \simeq 0.3\mu_{cr}$, the fundamental frequency monotonically decreases to zero, as typically predicted by the linear theory.

The pull-in parameters correspond to values of λ when the fundamental frequency of the deflected plate vanishes. Values of λ for which the lowest frequency approaches zero match with values of λ_{PI} obtained from the analysis of the static problem described above.

Results in Fig. 8 show that for $\alpha = 1$ and $\beta = 0$ the fundamental frequency monotonically decreases, meaning that in this case the softening effect related to the Coulomb and the Casimir forces overwhelms the strain hardening effect, induced by the stretching of the plate.

Pull-in parameters computed herein have not been compared with experimental data since none is available in the current literature.

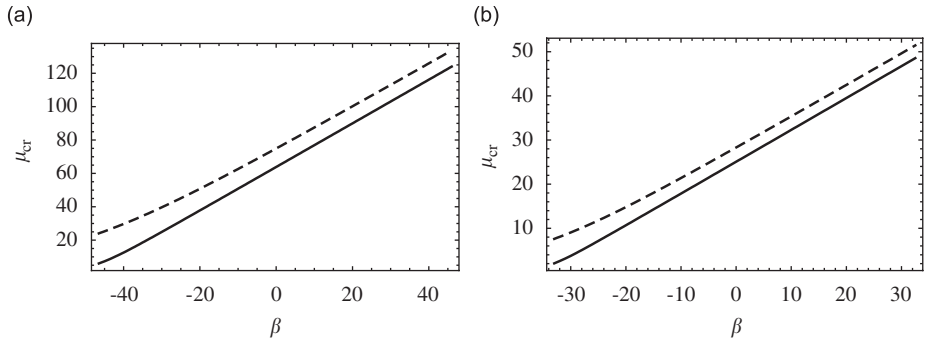

Fig. 9. For $\alpha = 1$ (solid line) and $\alpha = 4$ (dashed line), variation with β of the critical Casimir force parameter μ_{cr} for (a) $b/a = 0.5$, and (b) $b/a = 0.75$.

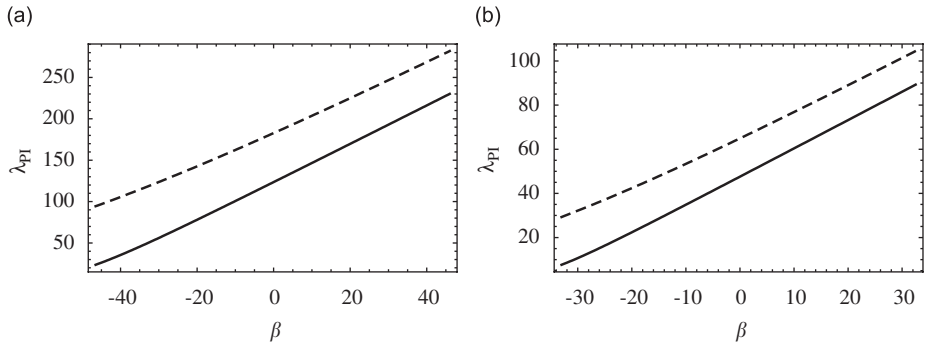

Fig. 10. For $\alpha = 1$ (solid line), $\alpha = 4$ (dashed line), and $\mu = 0$, variation with β of the pull-in voltage parameter λ_{PI} for (a) $b/a = 0.5$, and (b) $b/a = 0.75$.

5.3. *Effect of the residual stress on pull-in and critical Casimir force parameters*

In Fig. 9, we plot the variation with β of the critical Casimir force parameter μ_{cr} for two aspect ratios of the elliptic plate, and also two values of α. We recall that the parameter β in Eq. (15) is a measure of the uniform residual stress $\overline{\sigma}$ in the microplate. For each case examined, we observe that μ_{cr} increases with increasing tensile residual stress and decreases with increasing compressive residual stress. Indeed, from Eqs. (15) and (45), a positive increment of prestress increases the overall stiffness, whereas a negative increment decreases the overall stiffness. Thus, the residual stress affects the minimum size of the device that can be safely fabricated.

In absence of the Casimir force, that is, for $\mu = 0$, Fig. 10 exhibits the variation with the prestress parameter β of the pull-in voltage λ_{PI} for two aspect ratios of the elliptic plate, and also for two values of α. We note that magnitudes of the initial compressive and tensile prestresses are limited, respectively, by the buckling instability of the MEMS and the tensile strength of the material of the MEMS.

5.4. *Pull-in parameters for a membrane*

For a linear elastic membrane the equation

$$-\frac{1}{\chi}\frac{\partial^2 w}{\partial x^j \partial x^j} + \frac{\lambda}{\beta(1+w)^2} + \frac{\mu}{\beta(1+w)^4} = 0, \tag{56}$$

governing static deflection under the action of the Coulomb and the Casimir forces is derived from Eq. (14a) with the assumptions that $\alpha \ll 1$ (small displacements), and $\beta \gg 1$ (bending stiffness negligible as compared to the stiffness due to the residual stress). Consistent with the von Kármán plate theory, the additional

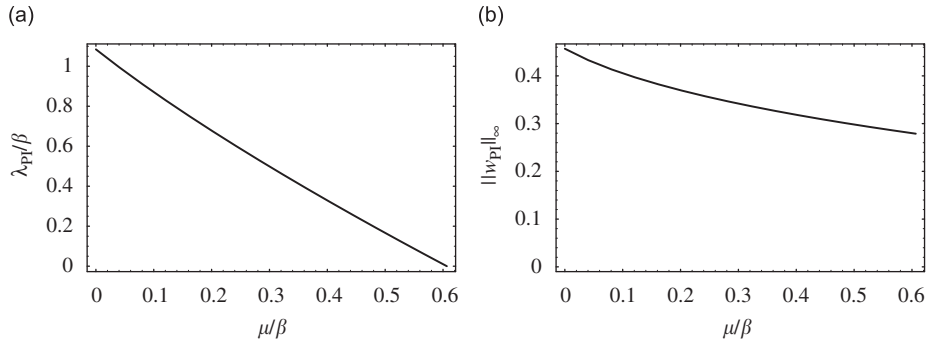

Fig. 11. For an elliptic clamped membrane with $b/a = 0.75$, pull-in parameters versus the Casimir force parameter.

Table 3
For the elliptic membrane and $\mu = 0$, comparison of pull-in parameters from the present one degree-of-freedom model with those obtained with the finite difference method in [29]

b/a	Finite differences [29]		Present work	
	λ_{PI}	$\|w_{PI}\|_\infty$	λ_{PI}	$\|w_{PI}\|_\infty$
0.25	6.257	0.4287	6.581	0.5049
0.50	1.912	0.4302	1.936	0.4665
0.75	1.073	0.4475	1.085	0.4575
0.95	0.8254	0.4368	0.8256	0.4562

hypothesis $g_0 \ll a$ and $h \ll a$ are implicit in the model. Therefore, the linear membrane approximation is applicable for microelectromechanical devices that experience small deflections and for which the bending stiffness is negligible as compared to the in-plane stiffness due to a constant prestress in carrying the external load. Eq. (56) shows that μ_{cr} varies linearly with β or, equivalently, that the ratio μ_{cr}/β is constant. The same remark applies to λ_{PI}/β for a given $\mu \in [0, \mu_{cr}]$. A reduced-order model for the linear membrane can be derived from Eq. (38) by setting $\mathbf{k}_1 = \mathbf{k}_3 = \mathbf{0}$, and by computing $\mathbf{m}$, $\mathbf{k}_2$, $\mathbf{f}_e$, and $\mathbf{f}_c$ in formulae listed as Eq. (39) with the nth basis function $w^m_{(n)}$ for the transverse displacement given by

$$\overline{w}^m_{(n)}(x^1, x^2) = A_n \mathrm{Ce}_0(x^1, q_{0n})\mathrm{ce}_0(x^2, q_{0n}), \quad n = 1, \ldots, N, \tag{57}$$

where A_n is a constant.

Pull-in parameters λ_{PI}/β and $\|w_{PI}\|_\infty$ versus $\mu/\beta \in [0, \mu_{cr}/\beta]$ are plotted in Fig. 11 for a clamped elliptic micromembrane ($b/a = 0.75$) by taking $N = 1$ in Eq. (57). They match very well with those obtained in Ref. [29] by solving the two-dimensional governing equation with the finite difference method using a grid of 50×70 points in the strip $[0, \mathrm{arctanh}(b/a)] \times [0, 2\pi]$. For $\mu = 0$, the non-dimensional pull-in voltage and the pull-in maximum displacement computed with the present one degree-of-freedom model are compared in Table 3 with those predicted by the finite difference method [29]. It is clear that the present method, by using only one degree-of-freedom for the transverse displacement, is able to reproduce within a good approximation results computed with 3500 degrees of freedom in the finite difference scheme.

The pull-in voltage for the elliptic membrane is considerably more than that for the circular membrane of radius equal to the major semi-axis of the ellipse. However, the pull-in deflection is essentially independent of the aspect ratio of the ellipse.

5.5. Remarks

In the literature, see for example Ref. [17], simple lumped models have been extensively used to analyze pull-in instability in MEMS. Despite being very simple, the accuracy of these models is often very limited. In what

follows we illustrate the application of the classical lumped model to the simplest case of a linear plate without initial stress and in absence of the Casimir force. In this case, the MEMS is modeled as a parallel plate capacitor, where both plates are rigid. The upper plate is suspended by a linear spring, and the bottom plate is held fixed. $\overline{\zeta}$ is the displacement of the upper conductor, and it represents the maximum value of the displacement w of the distributed system. The lumped one degree-of-freedom model is

$$-k\overline{\zeta} = \frac{\lambda}{(1+\overline{\zeta})^2}, \tag{58}$$

where k is the non-dimensional spring stiffness. The constant k may be computed by solving a sample static problem on the distributed system without the Coulomb force. Typically, a uniformly distributed load on the movable conductor is considered, see for example Refs. [44,36]. In this case, the stiffness k is equal to $1/\|w^\star\|_\infty$, where $w^\star$ is the solution in elliptic coordinates of the boundary value problem

$$\frac{1}{\chi}\frac{\partial^2}{\partial x^k \partial x^k}\left(\frac{1}{\chi}\frac{\partial^2 w^\star}{\partial x^j \partial x^j}\right)(x^1,x^2) = \frac{\Theta^4}{(1-\Theta^2)^2}, \tag{59a}$$

$$w^\star(x_b^1,x^2) = 0, \quad \frac{\partial w^\star}{\partial x^1}(x_b^1,x^2) = 0. \tag{59b}$$

The solution of Eq. (59) is, see for example Ref. [59],

$$w^\star(x^1,x^2) = \frac{(\cosh 2x^1 - \cosh 2x_b^1)^2(\cos 2x^2 - \cosh 2x_b^1)^2}{128(2+\cosh 4x_b^1)\sinh^4 x_b^1}. \tag{60}$$

Therefore

$$k = \frac{1}{\|w^\star(0,0)\|_\infty} = \frac{8(2+\cosh 4x_b^1)}{\sinh^4 x_b^1}. \tag{61}$$

By solving the equilibrium Eq. (58) along with the pull-in instability condition

$$k - \frac{2\lambda_{\mathrm{PI}}}{(1+\overline{\zeta}_{\mathrm{PI}})^3} = 0, \tag{62}$$

obtained by setting the overall tangent stiffness equal to zero, we obtain the following expressions for pull-in parameters from the lumped model

$$\overline{\zeta}_{\mathrm{PI}} = -\frac{1}{3}, \quad \lambda_{\mathrm{PI}} = \frac{4}{27}k. \tag{63}$$

By setting $\alpha = 0$, $\beta = 0$, and $\mu = 0$ in Eq. (38) we obtain the reduced-order model of a linear elliptic microplate without the prestress and without the Casimir force. We note that by setting $\alpha = 0$ there is no coupling between in-plane and transverse displacements. Therefore, the reduced-order model for the linear plate is independent of the number of basis functions for the in-plane displacement.

For $\alpha = 0$, $\beta = 0$, $\mu = 0$, and different aspect ratios of the elliptic plate, we compare in Table 4 the pull-in parameters of the linear plate computed with the lumped model and with the present reduced-order model

Table 4
For the linear elliptic plate ($\alpha = 0$) with $\beta = 0$ and $\mu = 0$, comparison of pull-in parameters from the present one degree-of-freedom model with those obtained with the lumped model in Ref. [17]

b/a	Lumped model [17]		Present work	
	λ_{PI}	$\|w_{\mathrm{PI}}\|_\infty$	λ_{PI}	$\|w_{\mathrm{PI}}\|_\infty$
0.50	69.9	0.333	109	0.477
0.75	19.0	0.333	43.1	0.471
0.95	10.5	0.333	17.2	0.471

with $N = 1$. The lumped model gives inaccurate results with respect to the converged solution of the reduced order model proposed in the paper, with the error for λ_{PI} as high as $\simeq 56\%$ when $b/a = 0.75$.

The reduced-order models presented herein can be employed to select among several possible designs of MEMS. The final few designs can then be thoroughly studied with a three-dimensional finite element (or any other) code to see if the pull-in parameters and the maximum stresses induced in the deformable plate stay within the design limit. The pull-in parameters under effects of the Casimir and the Coulomb forces for circular and rectangular plates have been studied by Batra et al. [62].

We note that the relation given by Eq. (12) for the Casimir force between two parallel plates is valid when the gap between the two plates exceeds 1 μm, see Ref. [33]. Thus results presented herein are valid for initial gap between the two plates of a few micrometers. For initial gaps of the order of a few nanometers, one needs to consider the van der Waals force rather than the Casimir force [33].

6. Conclusions

We have derived reduced-order models for clamped microelectromechanical von Kármán elliptic plates subject to both the Coulomb and the Casimir forces. The nonlinear governing equations for the three displacement components are coupled. Static pull-in parameter, and small vibrations about equilibrium configurations of a plate statically predeformed by the applied voltage and the Casimir force are analyzed. The first natural frequency rapidly drops to zero when the applied voltage approaches the pull-in voltage.

We have employed the Galerkin method using basis functions defined on the entire domain and satisfying prescribed kinematic boundary conditions. The method is meshless in the sense that no discretization of the domain is required. It is found that 20 basis functions for the in-plane displacement and 1 basis function for the transverse displacement give converged results. Because of the coupling between in-plane and transverse displacements, the number of degrees of freedom in the reduced-order model equals the number of basis functions for the transverse displacement. Accurate values of the pull-in parameters can be obtained with 6 basis functions for the in-plane displacements.

The reduced-order model for a plate is simplified to that for the corresponding membrane by neglecting the bending stiffness of the plate. Pull-in parameters for elliptic membranes from the one degree-of-freedom model are found to agree well with those obtained by solving numerically the complete set of governing equations with the finite difference method using 3500 grid points. Thus the present approach is considerably more computationally efficient.

Critical values of the Casimir force parameter for the elliptic plates and membranes have been determined. These give dimensions of MEMS that can be safely fabricated.

References

[1] C.T.C. Nguyen, L.P.B. Katehi, G.M. Rebeiz, Micromachined devices for wireless communications, *Proceedings of the IEEE*, vol. 86, 1998, pp. 1756–1768.

[2] E.S. Hung, S.D. Senturia, Extending the travel range of analog-tuned electrostatic actuators, *Journal of Microelectromechanical Systems* 8 (4) (1999) 497–505.

[3] R.K. Gupta, S.D. Senturia, Pull-in time dynamics as a measure of absolute pressure, *Proceedings IEEE International Workshop on Microelectromechanical Systems* (*MEMS'97*), Nagoya, Japan, 1997, pp. 290–294.

[4] P.B. Chu, P.R. Nelson, M.L. Tachiki, K.S. Pister, Dynamics of polysilicon parallel-plate electrostatic actuators, *Sensors and Actuators A* 52 (1996) 216–220.

[5] J.A. Pelesko, D.H. Bernstein, *Modeling MEMS and NEMS*, Chapman & Hall, Boca Raton, FL, 2002 (Chapter 7).

[6] E.M. Abdel-Rahman, M.I. Younis, A.H. Nayfeh, Characterization of the mechanical behavior of an electrically actuated microbeam, *Journal of Micromechanics and Microengineering* 12 (6) (2002) 759–766.

[7] A.H. Nayfeh, M.I. Younis, Dynamics of MEMS resonators under superharmonic and subharmonic excitations, *Journal of Micromechanics and Microengineering* 15 (2005) 1840–1847.

[8] J.F. Rhoads, S.W. Shaw, K.L. Turner, The nonlinear response of resonant microbeam systems with purely-parametric electrostatic actuation, *Journal of Micromechanics and Microengineering* 16 (2006) 890–899.

[9] H.A. Tilmans, R. Legtenberg, Electrostatically driven vacuum-encapsulated polysilicon resonators: part II. Theory and performance, *Sensors and Actuators A* 45 (1) (1994) 67–84.

[10] M.I. Younis, A.H. Nayfeh, A study of the nonlinear response of a resonant microbeam to an electric actuation, *Nonlinear Dynamics* 31 (2003) 91–117.
[11] S. Krylov, R. Maimon, Pull-in dynamics of an elastic beam actuated by continuously distributed electrostatic force, *Journal of Vibration and Acoustics* 126 (2004) 332–342.
[12] J.-H. Kuang, C.-J. Chen, Dynamic characteristics of shaped micro-actuators solved using the differential quadrature method, *Journal of Micromechanics and Microengineering* 14 (4) (2004) 647–655.
[13] W.C. Xie, H.P. Lee, S.P. Lim, Nonlinear dynamic analysis of MEMS switches by nonlinear modal analysis, *Nonlinear Dynamics* 31 (2003) 243–256.
[14] A. Singh, R. Mukherjee, K. Turner, S. Shaw, MEMS implementation of axial and follower end forces, *Journal of Sound and Vibration* 286 (2005) 637–644.
[15] J.F. Rhoads, S.W. Shawa, K.L. Turner, J. Moehlis, B.E. DeMartini, W. Zhang, Generalized parametric resonance in electrostatically actuated microelectromechanical oscillators, *Journal of Sound and Vibration* 296 (2006) 797–829.
[16] G.I. Taylor, The coalescence of closely spaced drops when they are at different electric potentials, *Proceedings of the Royal Society A* 306 (1968) 423–434.
[17] H.C. Nathanson, W.E. Newell, R.A. Wickstrom, J.R. Davis, The resonant gate transistor, *IEEE Transactions on Electron Devices* 14 (3) (1967) 117–133.
[18] H.A. Tilmans, R. Legtenberg, Electrostatically driven vacuum-encapsulated polysilicon resonators: part I. Design and fabrication, *Sensors and Actuators A* 45 (1994) 57–66.
[19] J. Pelesko, A. Triolo, Nonlocal problems in MEMS device control, *Journal of Engineering Mathematics* 41 (4) (2001) 345–366.
[20] S. Timoshenko, *Theory of Elasticity*, third ed., McGraw-Hill Companies, New York, 1970.
[21] O. Francais, I. Dufour, Normalized abacus for the global behavior of diaphragms: pneumatic, electrostatic, piezoelectric or electromagnetic actuation, *Journal of Modeling and Simulation of Microsystems* 2 (1999) 149–160.
[22] T.Y. Ng, T.Y. Jiang, K.Y. Lam, J.N. Reddy, A coupled field study on the non-linear dynamic characteristics of an electrostatic micropump, *Journal of Sound and Vibration* 273 (2004) 989–1006.
[23] X. Zhao, E.M. Abdel-Rahman, A.H. Nayfeh, A reduced-order model for electrically actuated microplates, *Journal of Micromechanics and Microengineering* 14 (7) (2004) 900–906.
[24] G.W. Vogl, A.H. Nayfeh, A reduced-order model for electrically actuated clamped circular plates, *Journal of Micromechanics and Microengineering* 15 (2005) 684–690.
[25] E.H. Mansfield, *The Bending & Stretching of Plates*, second ed., Cambridge University Press, Cambridge, New York, 1989 (Chapter 9).
[26] J.A. Pelesko, Mathematical modeling of electrostatic MEMS with tailored dielectric properties, *SIAM Journal of Applied Mathematics* 62 (3) (2002) 888–908.
[27] J.A. Pelesko, D.H. Bernstein, J. McCuan, Symmetry and symmetry breaking in electrostatic MEMS, *Proceedings of Modeling and Simulation of Microsystems*, San Francisco, CA, USA, 2003, pp. 304–307.
[28] J.A. Pelesko, X.Y. Chen, Electrostatic deflections of circular elastic membranes, *Journal of Electrostatics* 57 (2003) 1–12.
[29] R.C. Batra, M. Porfiri, D. Spinello, Analysis of electrostatic MEMS using meshless local Petrov–Galerkin (MLPG) method, *Engineering Analysis with Boundary Elements* 30 (11) (2006) 949–962.
[30] R.C. Batra, M. Porfiri, D. Spinello, Effects of Casimir force on pull-in instability in micromembranes, *Europhysics Letters* 77 (2007) 20010.
[31] S. Wong, C. Fox, S. McWilliam, Thermoelastic damping of the in-plane vibration of thin silicon rings, *Journal of Sound and Vibration* 293 (2006) 266–285.
[32] S.K. Lamoreaux, The Casimir force: background, experiments, and applications, *Reports on Progress in Physics* 68 (2005) 201–236.
[33] M. Bordag, U. Mohideen, V.M. Mostepanenko, New developments in the Casimir effect, *Physics Reports* 353 (2001) 1–205.
[34] E.M. Lifshitz, The theory of molecular attractive forces between solids, *Soviet Physics JETP* 2 (1956) 73–83.
[35] Y.-P. Zhao, L.S. Wang, T.X. Yu, Mechanics of adhesion in MEMS-a review, *Journal of Adhesion Science and Technology* 17 (4) (2003) 519–546.
[36] S. Pamidighantam, R. Puers, K. Baert, H.A.C. Tilmans, Pull-in voltage analysis of electrostatically actuated beam structures with fixed-fixed and fixed-free end conditions, *Journal of Micromechanics and Microengineering* 12 (4) (2002) 458–464.
[37] L.M. Castañer, S.D. Senturia, Speed-energy optimization of electrostatic actuators based on pull-in, *Journal of Microelectromechanical Systems* 8 (3) (1999) 290–298.
[38] Y. Zhang, Y.-p. Zhao, Numerical and analytical study on the pull-in instability of micro-structure under electrostatic loading, *Sensors and Actuators A: Physical* 127 (2006) 366–380.
[39] R.C. Batra, M. Porfiri, D. Spinello, Electromechanical model of electrically actuated narrow microbeams, *Journal of Microelectromechanical Systems* 15 (5) (2006) 1175–1189.
[40] R.C. Batra, M. Porfiri, D. Spinello, Vibrations of narrow microbeams predeformed by an electric field, *Journal of Sound and Vibration* 309 (3) (2008) 600–612.
[41] F.M. Serry, D. Walliser, G.J. Maclay, The role of the Casimir effect in the static deflection and stiction of membrane strips in microelectromechanical systems (MEMS), *Journal of Applied Physics* 84 (5) (1998) 2501–2506.
[42] J.-N. Ding, S.-Z. Wen, Y.-G. Meng, Theoretical study of the sticking of a membrane strip in MEMS under the Casimir effect, *Journal of Micromechanics and Microengineering* 11 (2001) 202–208.
[43] J. Bárcenas, L. Reyes, R. Esquivel-Sirvent, Scaling of micro- and nanodevices actuated by Casimir forces, *Applied Physics Letters* 87 (2005) 263106.

[44] W.-H. Lin, Y.-P. Zhao, Casimir effect on the pull-in parameters of nanometer switches, *Microsystem Technologies* 11 (2) (2005) 80–85.
[45] Y.C. Liang, W.Z. Lin, H.P. Lee, S.P. Lim, K.H. Lee, Proper orthogonal decomposition and its applications—part II: model reduction for MEMS dynamical analysis, *Journal of Sound and Vibration* 256 (3) (2002) 515–532.
[46] R.C. Batra, M. Porfiri, D. Spinello, Review of modeling electrostatically actuated microelectromechanical systems, *Smart Materials and Structures* 16 (2007) R23–R31.
[47] R.T. Howe, R.S. Muller, Resonant-microbridge vapor sensor, *IEEE Transactions on Electronics Devices* 33 (1986) 499–506.
[48] D.C. Abeysinghe, S. Dasgupta, H.E. Jackson, J.T. Boyd, Novel MEMS pressure and temperature sensors fabricated on optical fibers, *Journal of Micromechanics and Microengineering* 12 (2002) 229–235.
[49] M.I. Younis, E.M. Abdel-Rahman, A.H. Nayfeh, A reduced-order model for electrically actuated microbeam-based MEMS, *Journal of Microelectromechanical Systems* 12 (5) (2003) 672–680.
[50] L.D. Landau, E.M. Lifshitz, *Theory of Elasticity*, Pergamon Press, New York, 1986.
[51] R.M. Bowen, C.-C. Wang, *Introduction to Vectors and Tensors*, vol. 2, Plenum Press, New York, 1976.
[52] R.C. Batra, *Elements of Continuum Mechanics*, AIAA: American Institute of Aeronautics and Astronautics, Reston, VA, 2005.
[53] S. Krylov, S. Seretensky, Higher order correction of electrostatic pressure and its influence on the pull-in behavior of microstructures, *Journal of Micromechanics and Microengineering* 16 (2006) 1382–1396.
[54] M. Bordag, Casimir effect for a sphere and a cylinder in front of a plane and corrections to the proximity force theorem, *Physical Review D* 73 (2006) 125018.
[55] H. Gies, K. Klingmüller, Casimir effect for curved geometries: proximity-force-approximation validity limits, *Physical Review Letters* 96 (2006) 220401.
[56] L. Meirovitch, *Analytical Methods in Vibrations*, Macmillan, New York, 1967.
[57] M.W. McLachlan, *Theory and Application of Mathieu Functions*, Oxford University Press, London, 1947.
[58] O. Bochobza-Degani, D. Elata, Y. Nemirovsky, An efficient DIPIE algorithm for CAD of electrostatically actuated MEMS devices, *Journal of Microelectromechanical Systems* 11 (5) (2002) 612–620.
[59] Z.-Q. Cheng, R.C. Batra, Three-dimensional thermoelastic deformations of a functionally graded elliptic plate, *Composites: Part B* 31 (2000) 97–106.
[60] M. Porfiri, Vibrations of parallel arrays of electrostatically actuated microplates, *Journal of Sound and Vibration* (2008), doi:10.1016/j.jsv.2008.02.007.
[61] R.C. Batra, M. Porfiri, D. Spinello, Effects of van der Waals force and thermal stress on pull-in instability of microplates, *Sensors* 8 (2008) 1048–1069.
[62] R.C. Batra, M. Porfiri, D. Spinello, Reduced-order models for microelectromechanical rectangular and circular plates incorporating the Casimir force, *International Journal of Solids and Structures* 45 (2008) 3558–3583.